Journal Pre-proofs

Formulation of Spinel based Inkjet Inks for Protective Layer Coatings in SOFC Interconnects

Sathish Pandiyan, Ahmad El-Kharouf, Robert Steinberger-Wilckens

PII: S0021-9797(20)30777-3
DOI: https://doi.org/10.1016/j.jcis.2020.06.032
Reference: YJCIS 26529

To appear in: *Journal of Colloid and Interface Science*

Received Date: 19 April 2020
Revised Date: 30 May 2020
Accepted Date: 7 June 2020

Please cite this article as: S. Pandiyan, A. El-Kharouf, R. Steinberger-Wilckens, Formulation of Spinel based Inkjet Inks for Protective Layer Coatings in SOFC Interconnects, *Journal of Colloid and Interface Science* (2020), doi: https://doi.org/10.1016/j.jcis.2020.06.032

Formulation of Spinel based Inkjet Inks for Protective Layer Coatings in SOFC Interconnects

Sathish Pandiyan[1], Ahmad El-Kharouf, Robert Steinberger-Wilckens.

Centre for Fuel Cell and Hydrogen Research, School of Chemical Engineering

University of Birmingham, Edgbaston, Birmingham, B15 2TT, United Kingdom

Abstract

In this study, inkjet printing technology was adopted for the application of protective layer coatings on metallic Solid Oxide Fuel Cell (SOFC) interconnects. The study highlights the potential of the inkjet printing process to fabricate aqueous-based protective layer coatings over ferritic stainless steels, a novel, very flexible and low-cost approach to coating. The work presented focusses on the formulation of aqueous-based spinel particulate inks for the inkjet printing process using an electro-magnetic inkjet printer. An ink formulation route based on a two-stage ball milling technique was developed to produce a printable ink composition with Manganese Cobalt Oxide ($MnCo_2O_4$, MCO) and Manganese Cobalt Ferrite ($MnCo_{1.8}Fe_{0.2}O_4$, MCF) as the coating materials. The stability of the ink suspensions, and particle size distribution were studied and characterised using zeta and a particle size analysis, respectively. The flow properties of the inks were analysed using a conventional rheometer at shear rates 1 to 1000 s^{-1} and Piezo Axial Vibrator rheometer at higher shear rates (10^{-6} s^{-1}). Finally, the printability of the inks was assessed theoretically based on the Ohnesorge number, Z. The formulated MCO and MCF inks with ~ 25 wt.% solid loading exhibited Z values of 4.17 and 6.77, satisfying the printability criteria of the inkjet inks. The printability of the inks was demonstrated by printing them on stainless-steel substrates. The printed layers were free of any

[1]corresponding author: sathish.pandiyan@outlook.com, tel. +44 (0) 121 4145275

visible defects after heat-treatment. The demonstrated ink formulation procedure provides a guide for inkjet inks development with respect to inkjet printer requirements. Furthermore, the outlined methodology can be employed to fabricate protective and other coatings for any kind of metallic components such as bipolar plates and heat-exchangers.

Keywords: Inkjet printing, Metal oxide inks, Protective layer, Interconnects, SOFC, Spinel.

1. Introduction

Interconnects are an integral part of SOFCs, providing structural and electrical connection between the repeating single-cell units in a stack. Ferritic stainless steels (FSS) are currently considered as the standard metal interconnect material [1,2]. FSS with 17 to 24 % chromium content offers protection against corrosion by forming a protective oxide layer under SOFC cathode operating conditions [3]. However, the thermally grown oxide layer (chromia) formed during the operation of SOFC stacks leads to a continuous degradation in key properties of the FSS interconnect material. The growth of the chromia layer with time depletes the chromium reservoir in the steel, whilst the removal of volatile chromium species causes increased diffusion from the steel bulk material to the surface layer. Volatile chromium hydroxide reacts with the SOFC cathode layer material resulting in chromium poisoning. The lower conductivity of the oxide layer negatively affects the overall electrical resistance of the interconnect layer [4,5]. Several steps such as alloy modifications, surface treatments and application of protective/conductive coatings have been studied as mitigation methods to overcome the degradation effects in metallic interconnects. Alloy modification enhanced the oxidation resistance of the interconnects by slowing down the kinetics of oxide growth. FSS variants such as Crofer 22APU, Crofer 22H, or Sanergy HT, were specifically developed in view of reducing high temperature corrosion and offer optimised alloy compositions for SOFC interconnect application [6]. However, alloy modification does not solve the volatilisation of

chromium species from the oxide layer during long-term operation. The application of protective and conductive coatings has shown significant results in further mitigating removal of volatile chromium species from the oxide layer. Also, offers improved conductivity by decelerating the growth of the oxide layer by slowing down the ingress of oxygen and outward migration of chromium species [6].

Different coating techniques can be broadly classified as Vacuum Deposition techniques and Wet Chemical methods. Vacuum Deposition processes such as Physical Vapour Deposition (PVD), Chemical Vapour Deposition (CVD), Electrodeposition and others. These techniques produce dense coating layers, but the limitation is in the thickness of the layer produced. As thin layers, these coatings fail to form a complete barrier against Cr species migration. Electrodeposition is one of the widely used approaches in recent years and has shown promising results in terms of oxidation resistance and Cr inhibition [7]. This technique is limited due to the interdiffusion of coating components into the substrate during oxidation, resulting in breakaway oxidation. The process also requires intensive sequential steps during the coating process. PVD has been very successful in producing very thin, dense coatings. Nevertheless, the use of vacuum chambers would inhibit large-scale industrial employment. Sandvik Materials Technology, though, has commercialised PVD-treated sheet materials . Wet Chemical methods such as slurry coating, wet powder spraying, and screen printing are well-known conventional processes in ceramics processing. Sol-gel, dip and spin coating are also applicable to interconnect protective layer application. These techniques are inexpensive and capable of coating large structures of varying thickness in short periods. However, they produce porous coating layers, often with non-uniformity across the layers. They also require masking, and a large amount of coating material is wasted during the process by overspray. Thermal Spray methods such as Vacuum Plasma Spraying (VPS) and Atmospheric Plasma Spraying (APS) form dense coatings but these are generally quite thick. Hu et al. [8] showed that the use

of APS in deposition of the spinel ($Mn_{1.5}Co_{1.5}O_4$) along with preheating and reactive sintering produced gas-tight protective layers and prevented Cr outward migration. Though APS produces more dense layers in comparison to the conventional plasma spraying technique, both require masking and are considered to be an expensive approach. As a batch process, similar to vacuum chamber PVD, VPS and APS do not easily lend themselves to industrial mass production. The primary challenges encountered in most of the coating methods are the requirement of masking, reproducibility, time consumed, integration into continuous industrial manufacturing, wastage of materials, and reducing the porosity in the layers applied.

With regards to the coating materials, spinel coatings have received significant attention [9,10]. Different spinel compositions have been analysed to find optimal protective-conductive layers for SOFC interconnects with low oxidation rate, low contact resistance, low electrical resistance, high adhesion, and, above all, low release rates of chromium [11–13]. Larring and Norby proposed $(Mn, Co)_3O_4$ as the promising candidate for the protective layer application for metallic SOFC interconnects (CFY alloy) [14]. Among different compositions in the system, $MnCo_2O_4$ and $Mn_{1.5}Co_{1.5}O_4$ have been widely studied in the recent decade [11,15–19]. However, the performance of the mentioned spinel compositions was improved by the substitution of Co with Fe and Cu . Addition of Fe and Cu in $MnCo_2O_4$ spinel system has shown an improved coefficient of thermal expansion (CTE) matching better with that of the ferritic stainless-steel substrates and with higher electrical conductivity, respectively [12,19,20]. The thermal behaviour of ferrite substituted into spinels has been studied in other contexts [21]. Detailed reviews on different coating materials and the coating techniques are reported in the literature authored by Shaigan et al. [22] and Mah et al. [23].

Inkjet printing (IJP) is an economical Wet Chemical deposition technique where inks are printed over the target substrate in any desired pattern. Based on the mode of operation, inkjet printing is classified into different types, namely, Continuous and Drop-on-Demand inkjet

printing (DOD). In DOD mode, ink droplets are ejected at pre-determined positions which eliminates the need for masking, even over 3D structures. The accuracy in placement and versatile drop generation has favoured the DOD mode of printers in various research and development sectors [24]. The prime challenge with inkjet technology is the formulation of ink that satisfies the selected mode of printing. The right choice of additives is significant to meet the ink rheological requirements such as viscosity and surface tension for efficient printing [25]. For instance, in recent years, IJP has been more scarcely used for the deposition of inorganic materials as compared to organic materials. This was mainly due to the challenges in synthesising inorganic inkjet inks due to their starting powder size (in the sub-microns to microns range) which could lead to clogging of nozzles and the requirement of stringent control over the particle size distribution.

Applying inkjet printing as a Wet Chemical method to produce SOFC interconnect protective coatings would combine several advantages:

- lack of requirement to mask the target,
- low-cost and versatile application of layers,
- use of aqueous-based inks, and
- swiftness and flexibility of the printing process.

There are also a number of drawbacks, such as the necessity to heat-treat the applied layers in order to increase the density, control over the viscosity, surface tension and the potential for clogging of the printing nozzles. These were among the challenges addressed in this study.

In general, inkjet inks are classified into four major types: solvent-based, aqueous-based, phase-change, and UV curable [26]. Solvent-based and aqueous-based inks are widely used in research applications whereas the other two types are employed mostly in commercial contexts such as the printing industry and media. Solvent-based inkjet inks are prone to clogging of the

nozzle due to the rapid evaporation of solvent leaving the solid particles at the nozzle. They also release volatile organic compounds and require a well-ventilated workspace. Despite the high surface tension, aqueous-based inks have gained attention as they are more environmentally friendly and have the option of using co-solvents such as alcohols to match the inkjet printer requirements [27–29].

X. Liu et al. [30] reviewed different ink formulation approaches for the inkjet deposition of functional metal oxide systems, namely: colloidal suspensions, sol-gel inks, and metal salt solutions. To achieve successful inkjet deposition of aqueous-based colloidal suspensions, the following considerations were proposed:

- For micron-sized metal oxide particles, an inkjet printer with a large nozzle (50 to 140 μm) should be chosen,
- Chemical methods such as sol-gel processing, hydrothermal or microwave synthesis, or mechanical methods such as ultrasonic mixing or ball milling should be used in formulating metal oxide inks.

Güngör et al. studied the effect of micronisation on three ceramic pigments, spinel, rutile, and zircon by mechanical milling for inkjet printing on ceramic tiles in terms of rheological and physical properties [31]. The major challenge with colloidal suspensions is their particle size distribution and stability of the suspended particles. The tendency of a suspended particle to flocculate may lead to sedimentation and, as a consequence, the clogging of the inkjet nozzle. As a rule of thumb, the particle size must be maintained below 10% of the IJP nozzle diameter, and the estimated optimal value is less than 2% with a narrow size distribution [30,32]. Also, the colloidal suspension must be stable to prevent particle flocculation with respect to time. The ink formulation and selection of ink components are merely dependent on the mode of

inkjet printer used. The essential components of inkjet inks are functional material, carrier medium and the additives.

Research studies have been carried out on inkjet deposition of functional coatings in ceramics[33–35], electronics/conductive structures [36–38], energy storage devices [39,40], sensors [41–43], and biological membranes [44–46]. Drop-on-Demand based printers have been used for the fabrication of functional layers in SOFC manufacturing [24,47–50]. To the best of our knowledge, inkjet printing technology has not been employed and studied for the application of protective layer coatings over metallic SOFC interconnects. The objective of the present work is to formulate aqueous-based spinel inks using sub-micron sized spinel powders with respect to the requirements of an electromagnetic printer. Printability of the inks was assessed based on the Reynolds-Weber space parameters. The selection of ink components and factors such as pH, stability of the ink, viscosity, surface tension, solid loading, rheological properties were studied. Ink formulation route based on two-stage ball milling method was developed.

2. Materials and Methods

2.1 Materials

Spinel powders Manganese Cobalt Oxide $MnCo_2O_4$ (MCO) and Manganese Cobalt Ferrite, $MnCo_{1.8}FeO_4$ (MCF) from Kceracell, South Korea, were used as coating materials. The mean particle size of the MCO and MCF powder as provided by the supplier were 0.54 and 0.55 microns, respectively. The steel substrate, K41 was used as the substrate material for printing the spinel inks as protective layer. The steel substrates were ultrasonicated in acetone bath for 15 minutes and wiped with ethanol prior to the printing process.

Darvan C-N (R.T Vanderbilt Company, Inc. USA) ammonium polymethacrylate (PMMA-NH_4) solution was used as the dispersant. Darvan C-N is known to dissociate in aqueous media before being absorbed into the surface of the dispersed particles. Poly Vinyl Alcohol (PVA) (Sigma Aldrich, UK) was used as the binder in the ink formulations. PVA comprises of polar OH^--groups which have a greater affinity and interaction with polar solvents such as water. Also, the use of water-soluble binder eliminates the variation of pH in the ink compositions. Polyethylene glycol (PEG) from Sigma Aldrich, UK, was used as a plasticiser in the ink, owing to its compatibility with the PVA. Glycerol (Sigma Aldrich, UK) was used as a lubricant in the inks to retain moisture and to prevent drying of inks at the ink nozzle. Surfactant, 2,4,7,9-Tetramethyl-5-decyne-4,7-diol ethoxylate (Sigma Aldrich, UK) was used to lower the surface tension of the water-based inks. Antifoam 204 (Sigma Aldrich, UK), a mixture of organic non-silicone-based polyether dispersions, was added to the formulation to eliminate air bubbles formation during the milling process. The physical properties of the dispersant, binder and other additives used for the ink formulation are given in the supplementary section, ST 1.

2.2 Methods

2.2.1 Ink formulation route

Aqueous based spinel inks based on different spinel powders were prepared by a two-stage milling process in a PET bottle with zirconia beads of 0.3 mm diameter as the grinding media. A comminution process ball milling technique was employed to break down the soft agglomerates and to attain a homogenous mixture of the different ink components. In the first milling stage, spinel powders suspended in DI water along with the dispersant and grinding media were ball milled for 24 hours at 400 rpm. Prior to the addition of powder, DI water and dispersant were milled for 10 to 15 minutes to ensure the dissolution of the water-soluble dispersant molecules. The binder solution was freshly prepared prior to the second milling

stage. Along with the binder solution, other additives such as plasticiser, surfactant, and, anti-foaming agent were added. The mixture was then subjected to slow milling at 200 rpm for 4 hours to achieve homogenous mixing. Inks were filtered and stored for further experimental studies. Fig. 1 shows the step-by -step procedure followed for optimisation of different ink components to achieve printable spinel inks.

Initially, the pH range for the ink formulation was determined using zeta analysis, as using a pH greater than 9 was prone to corrode the inkjet nozzles. In order to avoid agglomeration of particles in the ink suspension, the iso-electric point of the inks was determined using Zeta analysis, and the pH value was maintained in a defined range during the optimisation of each ink component. The optimal dispersant dosage to maintain ink stability and to understand the effect of milling time for different dispersant dosages was analysed using particle size distribution data. The effective dispersant dosage itself was analysed using a sedimentation test. With the optimal pH, milling time and dispersant dosage, the effect of different binder concentration was established using flow curve analysis. To understand the interaction between the dispersant and binder molecules, the binder concentration was varied at low and high dispersant dosages. The effective binder content was then determined based on the target viscosity values. Finally, the solid content was varied, and the optimal content was determined based on viscosity values. Based on the optimal dispersant, binder, and solid content, final inks were formulated, and their physical properties were identified to assess the printability of the inks using the dimensionless numbers, Reynolds (Re) and Weber number (We).

2.2.2 Zeta analysis

A zeta sizer Nano Z (Malvern Panalytical) was used in this study to determine the Iso-Electric Point (ISE) of spinel powders to find the stable pH region for the ink formulation. 0.1 g of the respective powders was added to 50 mL distilled water and agitated using a stirrer plate to

obtain the base sample. A 10 mL quantity from the base sample was extracted, and the pH was modified by adding a few drops of a 0.1 M solution of nitric acid and ammonia. The pH was monitored using a pH meter. The titrated sample was then fed into a DTS070 folded capillary cell for zeta analysis.

2.2.3 Particle Size analysis

A Mastersizer 2000 (Malvern Panalytical) was used to determine the particle size distribution (PSD). The inks were subjected to varying dispersant dosage and milled for 24, 48 and 72 hours to identify the optimal milling time and the effect of varying dispersant dosages. The optimal dispersant concentration and milling time for the ink formulation were determined by studying the effect of different milling time on PSD at varying amounts of dispersant dosage. Dispersant dosage of 0.25 ml for 5 gram of powder will be represented as 5 wt.% in the following. The optimal milling time was determined based on the evolution of d_{50} (mean particle size) and d_{90} (maximum particle size) values from the PSD data. This analysis was done on day 0. Samples were stored for ageing for a week (day 7) and were not agitated or stirred during the aging time. The PSD analysis to observe the sedimentation behaviour of the suspensions at different dispersant dosages was conducted on day 7.

2.2.4 Rheology

A Discovery HR-2 rheometer (TA Instruments) was used to determine the rheological behaviour of the inks. Flow curve analysis was carried out to identify optimal dispersant dosage, binder and solid content with respect to the inkjet printer used in the study. The measurements were performed using a sandblasted 40 mm parallel-plate geometry in the shear interval of 1 to 1000 s^{-1}. Prior to the measurement, samples were subjected to pre-shear of 100 s^{-1} for 60 seconds. The measured rheological data were fitted with an available rheological model to identify the effect of varying dispersant dosage on flocculation and to elucidate the

flow properties of the formulated spinel inks. The viscoelastic behaviour and complex viscosity of the inks with the final compositions were then analysed using the Piezo-Axial Vibrator (PAV), dynamic squeeze flow rheometer (Rheology centre, Department of Chemical Engineering and Biotechnology, University of Cambridge) .

2.2.5 Inkjet printer

The inkjet printer used for the deposition process was based on electromagnetic printing technology, referred to as valve-jet technology. The custom-made inkjet printer was composed of an electromagnetic single nozzle printhead with the opening of 90 μm mounted directly above the substrate on a Roland pen plotter. The image of the inkjet printer used is the present study is given in supplementary material, Fig S1. The electromagnetic solenoid valve connected to the ink reservoir was closed by a rubber-tipped piston. The piston was driven up and down (opening and closing the orifice) as a consequence of the magnetic field generated in the solenoid when a pulse of current was applied. The period of the pulse, termed as "opening time", controlled the time for which the orifice was left open and thereby ensuring a controlled volume of the ink was ejected through the nozzle to form the droplet [48]. The ink reservoir was separated from the external solenoid, and thus the heat generated at the solenoid did not affect the inks, assuring that the viscosity of the ink suspension remained constant.

3. Results and Discussions

3.1 Determination of Iso-Electric Point

The isoelectric point (IEP) of the spinel powders in aqueous suspension is the point at which the surface charge of the particle is neutral. At IEP, suspended particles tend to attain thermodynamic equilibrium resulting in an onset of flocculation that leads to sedimentation with time [51]. Also, it is crucial to determine the IEP within a defined pH range, corresponding to the inkjet printer requirement, for instance, a pH greater than 9 is prone to corrode the inkjet

nozzles and would therefore not be considered. The IEP value for MCO and MCF powder suspension in distilled water was found to be in the pH range 2.0 to 3.0, as shown in Fig. 2.

Metal oxides dispersed in an aqueous medium, due to their amphoteric nature, dissociate as weak bases or acids resulting in the formation of H^+ and OH^- ions as shown in Equations (1) and (2). MCO and MCF powders exhibited positive Zeta values in acidic conditions below the IEP, and negative Zeta values above the IEP, due to the protonation and deprotonation of the hydroxy group in acidic and basic conditions, respectively. The observed amphoteric nature of the spinel powders is a common characteristic of metal oxides, as reported in the literature [52–54]:

$$M-OH \leftrightarrow M-O^- + H^+ \text{ (in basic conditions)} \quad (1)$$

$$M-OH + H^+ \leftrightarrow M-OH_2^+ \text{ (in acidic conditions)} \quad (2)$$

The ion concentration, which acts as a function of pH in the suspension, directly influences the surface charge of the dispersed particles and the Zeta potential [55], signifying the pH as a critical factor in dispersion stability. Thus, the pH for the inks formulated was maintained within the pH range 8.0 to 8.5, to ensure that the pH operating range was away from the IEP and to enhance the dissociation of the selected anionic dispersant selected.

3.2 Effect of milling time

Fig. 3 shows the d_{50} and d_{90} values obtained from PSD analysis of MCO suspensions measured each after 24, 48, and 72 hrs milling time at varying dispersant dosages. After 24 hrs of milling time, the d_{50} value was comparable to the manufacturer value (0.5434 μm). Fig. 4 shows the d_{50} and d_{90} values of MCF suspensions measured after 24, 48, and 72 hrs milling time at varying dispersant dosages. After 24 hrs of milling time, the d_{50} value at dispersant dosages above 10 wt.% was less than 0.45 μm, less than the manufacturer value (0.5521 μm). There was no

significant trend observed after 48 hrs and 72 hrs of milling, where d_{50} and d_{90} for MCO and MCF were less than 0.4 and 1.0 microns, respectively. For both ink suspensions (MCO and MCF), the maximum decrease in particle size d_{50} and d_{90}, was seen after 72 hrs at the dispersant dosages above 20 wt.%. The comminution process (ball milling technique) used in the present study was applied in order to obtain a homogenous ink suspension and break down any soft agglomerates. The best reduction in PSD was achieved with a maximum milling time of 72 hrs. However, when varying dispersant dosage, after storage (day 7) an increase in PSD was seen in both the inks for the samples milled 48 and 72 hrs whereas 24 hrs milled samples remained consistent. The observed increase in PSD could be attributed to the increase in surface area of particles after 48 and 72 hrs milling at day 0, demanding more dispersant concentration to prevent them from flocculating. The weakening of colloidal stability in ceramic pigments due to prolonged milling has been reported in similar work on inkjet printability of aqueous based ceramic inks [56]. Hence, the effect of dispersant dosage was evaluated for 24 hrs milled samples based on the evolution of d_{90} on each sample after 7 days of ageing.

Fig. 5 shows the images of the ink suspensions left for stability analysis on day 0 and day 7. At low dispersant dosages (10 and 20 wt.%) clear settling of particles can be seen for both the inks, where MCF suspensions showed quicker settling than the MCO suspensions. In the case of MCO ink suspensions, supernatant of the stored inks showed the presence of particles at the dispersant dosage 30 and 40 wt.% after ageing whereas in MCF ink suspensions it was observed at 40.wt% dispersant dosage.

MCO and MCF ink suspensions milled for 24 hrs displayed the maximum particle size within the requirements of the inkjet printer (less than 2 μm). Based on the PSD, and sedimentation test, 40 wt% dispersant dosage to the solid content was selected for the further formulation.

3.3 Optimal dispersant dosage and the flow curve response of ink suspensions

The dynamic viscosity of the ink suspensions milled for 24 hours at different dispersant dosages is shown in Fig. 6 (a-b). The viscosity of the ink suspensions decreased with the applied shear rate, as expected, due to the presence of polymer molecules and flocculation. The observed shear-thinning behaviour is a typical characteristic of suspension-based systems. Similar behaviour has been reported for other ceramic and metal-oxide suspension systems [57–59]. As a general trend, MCO and MCF inks showed a decrease in viscosity with respect to the increase in dispersant dosage. The observed lower viscosity reflected the lower resistance to flow, indicating less flocculation as the dispersant dosage increased from 5 to 40 wt.%. The measured dynamic viscosity of the inks with different dispersant dosages at the shear rates 1 s^{-1} and 1000 s^{-1} is shown in Table 1.

In both cases, viscosity values were less than 5 mPa.s, and the rate of increase was of a small magnitude. Thus, the degree of flocculation at different dispersant dosages was determined by fitting the measured flow curves with the Herschel-Bulkley equation to obtain the apparent yield stress. The presence of flocs or network structure in the suspension requires higher yield stress relative to the less flocculated suspension. In the literature, a similar approach was adopted to estimate the effect of polyelectrolyte on the flocculation [60,61]. The best rheological fit was obtained by the Herschel-Bulkley model equation with an R^2 value above 0.99 for each sample. The low yield stress values for MCO and MCF inks were above 30 wt.% solid loading, highlighting the lower flocculation tendency in the ink suspensions, which agreed well with the viscosity values and the sedimentation stability results. The yield stress values for MCO and MCF inks at different dispersant dosages are given in supplementary material, ST2.

3.4 Optimisation of the binder content

The addition of binder acts as a viscosity modifier and primarily affects the rheology of the suspension. It is important to determine the optimal binder concentration that maintains the viscosity within the desired value for the inkjet deposition process. Having set the optimal pH, dispersant dosage and milling time, varying binder concentrations were analysed based on the flow curve analysis with a target viscosity value of less than 15 mPa.s. To understand the interaction of the binder and the dispersant, a low dispersant dosage (LD=5wt.% dispersant) and a high dispersant dosage (HD=40wt.%) were chosen, and the concentration of the PVA solution was varied. The PVA concentration was limited to 15wt.% as higher loading which yielded a viscosity beyond the target viscosity (15 mPa.s).

Fig. 7 (a-b) shows the flow curve analysis of varying binder concentrations for the different dispersant dosages for MCO and MCF ink suspensions, respectively. Table. 2 shows the measured dynamic viscosity at the shear rates 1 s^{-1} and 1000 s^{-1} for varying binder concentrations at the respective lower and higher dispersant dosages. It can be seen that the viscosity increased when binder content was varied at lower dispersant dosage whereas, in the case of high dispersant dosage, the variation of viscosity with respect to binder content was minimal for both inks. 10 wt.% binder with 40 wt.% dispersant resulted in a lower viscosity value for both inks.

The increase in viscosity with respect to the increase in binder content was due to the presence of Darvan C-N molecules. Darvan C-N, a polymer of high molecular weight, extends into the suspending medium with a tail-loop configuration, causes entanglement with the binder molecules and exhibits a shear-thinning behaviour [62], as observed in the case of ink suspension. Khan et al. showed that the addition of PVA in the presence of a dispersant, in that case Darvan C, significantly affected the rheology of aqueous-based alumina suspensions [63].

However, the less pronounced effect on viscosity at higher dispersant concentration can be due to the weakened lubricant characteristics of Darvan C-N. The excess of Darvan C-N molecules at higher dispersant dosage easily breaks down into smaller chains during the milling stage and acts as lubricant between the polymeric chains of binder molecules, thereby reducing the flow resistance [58]. Nampi et al. [64] showed that the effect of PVA binder was less pronounced with the addition of stearic acid which acted as internal lubricant in alumina-based suspensions for spray coating application. The interaction between the binder and the suspended particles is considered to be lower at the optimal pH and dispersant concentration [65].

3.5 Effect of solid loading on the viscosity of the ink suspensions

Fig. 8 (a-b), shows the effect of solid content on the viscosity of the ink suspensions. The optimal solid loading was investigated with reference to the target viscosity to attain a maximum dense layer post inkjet deposition process. The viscosity of both the MCO inks remained less than 10 mPa.s at 30 and 35 wt.% solid loading, whereas, in the case of the MCF ink, the viscosity value was higher than the target viscosity at 35 wt.% solid loading. The increase in solid content led to increased volume fraction of particles in the suspension. As a consequence, the particle-particle interaction became dominant and more resistance to flow was observed in the form of an increase in the viscosity.

Table. 3 shows the measured dynamic viscosity of MCO and MCF ink suspensions for different solid content at the shear rates 1 s^{-1} and 1000 s^{-1}. MCF ink displayed a viscosity greater than 15 mPa.s at 35 wt.% whereas MCO ink showed comparatively lower viscosity. At 30 wt.% solid loading, both inks had a viscosity within the targeted value of less than 15mPa.s, and therefore this loading was chosen for the final ink compositions. Therefore, the ball-milling based ink formulation route allows to achieve solid loading of 30 wt.% (without other additives) at this stage.

3.6 Optimised spinel ink composition and characterisation

The final composition of the MCO and MCF inks with optimal milling time of 24 hrs, dispersant, binder, solid loading, and other additives based on the adapted ink formulation route is shown in Table. 4. The physical properties and jet-ability of the inks were assessed prior to the inkjet deposition process. Moreover, the wettability of the inks with the steel substrate was analysed using contact angle measurements, and the thermo-gravimetric analysis was performed before the heat-treatment step of the inkjet-printed samples.

3.6.1 PSD

The optimised inks displayed monomodal distribution without any agglomeration or secondary peak, as shown in Fig. 9. The measured d_{90} values for MCO and MCF inks were 1.29 ±0.017 and 1.05 ±0.003 µm, respectively. The maximum particle size observed was less than 2% of the inkjet printer nozzle size , making the achieved PSD well within the range of inkjet printer requirements used in the present study. The stability of the inks was assessed based on the PSD data measured on day 0 and after 7 days. Table 5 shows the PSD data of the spinel inks on day 0 and day 7. The increase in d_{50} and d_{90} on day 7 signifies the onset of flocs, yet the maximum particle size did not exceed 2 microns. The maximum particle size of the formulated MCO and MCF inks were 1.4 and 1.1% respectively, which is less than the critical value (2% of the nozzle size) to avoid clogging of the nozzle [32]. Thus, formulated inks could be stored and used for the inkjet deposition process at a later date.

3.6.2 Flow curve

The flow curve analysis for both inks is shown in Fig. 10. The inks exhibited shear-thinning behaviour, a characteristic behaviour for ceramic suspensions [65–67]. The change in viscosity with respect to the shear force in the formulated inks could be attributed to the structural alignment of polymers in the suspension and the particulate matter. Whereas, at the low shear

rate, the observed high viscosity was a result of more resistance exerted by the smaller particles which are in constant Brownian motion [62]. The MCO and MCF inks had viscosities of 72.1 and 53.32 mPa.s at the shear rate of 0.01 s^{-1}, and 9.98 and 11.26 mPa.s at the shear rate of 1000 s^{-1}, respectively. The high viscosity at low shear rate (<1 s^{-1}) offered kinetic stability to the suspended particles against the gravitational force during storage and ensured better stability. Although the measured viscosity was high at low shear rate (0.1 s^{-1}), both inks attained the viscosity value of ~15 mPa.s at medium shear rate (10 s^{-1}) which was equal to the shear force at the time of droplet delivery at the inkjet printer nozzle. Therefore, the achieved ink viscosity was well within the requirements for the printing process.

The rheological parameters for the inks were determined by fitting the measured data of shear rate against viscosity with available rheological models, shown in Fig. 10. The best fit was shown by the Carreau-Yasuda model with an R^2 value of 0.98 and 0.99 for MCO and MCF inks, respectively (values of the data fit is given in supplementary material, ST 3). The model used was a generalised form of Carreau's model, describing the characteristics of shear-thinning fluids. The Carreau-Yasuda model is represented by Equation 3,

$$\frac{\eta - \eta_\infty}{\eta_o - \eta_\infty} = [1 + (k\gamma)^a]^{\frac{n-1}{a}} \quad (3)$$

where η_o is zero shear viscosity, η_∞ is the infinite rate viscosity, k is the consistency, n is the power-law index representing the transition between η_o and the power-law region. The power-law index is used to elucidate the flow behaviour of the fluids, n less than unity signifies the shear-thinning characteristic of the inks.

3.6.3 Viscoelastic behaviour

In general, inkjet inks are characterised based on the flow curve analysis to understand the rheological behaviour and the resistance to flow. Practically, the test conditions do not reflect

the real-time printing process where the shear force experienced by the inks is in the order of ~10^{-6} s^{-1}. The stability of the formulated ink suspensions was assessed using a PAV rheometer at the frequency ~5Hz, replicating the shear force during the inkjet process. The viscoelastic moduli, storage modulus (G') and loss modulus (G''), were measured in the frequency range 30 Hz to 5 kHz, as shown in Fig. 11(a). G' and G'' represent the measure of elastic and viscous resistance to deformation, respectively [68]. It is evident that both inks exhibit viscoelastic liquid nature, with dominant G'' throughout the measured frequency. This behaviour indicated the suspension was stable with particles separated from each other irrespective of the frequency applied. Similar characteristics were reported for stable aqueous-based silver ink suspensions at higher frequencies in [69]. The drop seen in G' at high frequency for the MCO ink is due to an artefact during the testing process. Fig. 11(b) shows the plot of complex viscosity against the shear rate for the inks with and without the methanol added to the ink suspensions. The measured complex viscosity was slightly higher than the dynamic viscosity exhibiting similar slight shear-thinning behaviour. Thus, the flow behaviour and viscoelastic property of the formulated spinel inks during inkjet printing process has been reported. The viscoelastic properties of the inkjet inks determine the droplet formation and break-up during the printing process, combined with filament stretching experiment droplet formation and break-up, can be studied in detail [70].

3.7 Printability of the spinel inks

The printability of the inks was assessed based on the Re-We space parameter. Table. 5 lists the measured physical properties of the formulated spinel inks. The printability of the formulated inks was assessed using Reynolds (Re) and Weber (We) numbers based on the semi-empirical model for the Re-We space parameter given in the Equations 4 to 6. Fromm [71] defined the parameter Z as the inverse of the Ohnesorge number, which rates inertial and

surface tension forces with viscous force. Fromm proposed that for stable droplet generation in DOD systems, Z must be greater than 2, which was further investigated by Reis and Derby [72] using numerical simulation. For successful inkjet deposition of ceramic suspensions, Z must lie within the limits $1 < Z < 10$ for satellite free drop generation, where the lower limit represents high viscosity and the upper limit relates to the surface tension force for formation of satellite droplets [73,74].

$$Re = \frac{v\rho a}{\eta} \tag{4}$$

$$We = \frac{v^2\rho a}{\gamma} \tag{5}$$

$$Oh = \frac{\sqrt{We}}{Re} = \frac{\eta}{(\gamma\rho a)^{\frac{1}{2}}} \tag{6}$$

where ρ, η and γ are the density, dynamic viscosity, and surface tension of the fluid, respectively, v is the velocity, and a is the characteristic length (the nozzle size of the printer used, in this case 90 μm). The measured physical properties for the spinel inks are shown in Table 6.

The inverse Ohnesorge number (Z) plotted against the Re-We space parameters for both the spinel inks is shown in Fig. 12. It can be seen that the inks lie well within the printable region with Z values of 6.17 and 4.77 for MCO and MCF inks, respectively. The ink formulation procedure allows identifying the printability of the inks using the Re-We space parameter prior to the real time inkjet printing process.

3.8 Inkjet deposition

The printability of the formulated inks was tested using an electromagnetic printer. The printing controlling parameters were (i) pressure; (ii) opening time, and (iii) line spacing (distance between the centres of two adjacent drops). The ejection of the ink droplets through the nozzle

was controlled by the pressure applied to the ink reservoir, and the volume of the droplets was determined by the nozzle opening time. The printing parameters were adopted based on previous work for the inkjet deposition of ceramic suspensions using the same electromagnetic printer [47,48,75]. The printing parameters used for the deposition of the formulated inks is given in supplementary material, ST4.

The inks were printed onto the ferritic steel substrate (K41 steel substrate), then subjected to heat treatment in air at 800°C for 10 hours with a heating and cooling rate of 5°C/min. Fig. 13 shows the steel substrates printed with MCO and MCF inks after the heat-treatment process. The inkjet-printed coating layers were free from any visible cracks post deposition and heat-treatment process.

4. Conclusions

Aqueous based spinel inks were successfully formulated, and the printability of the inks was assessed based on the Re-We parameter. The effect of milling time and different dispersant dosage for the sub-micron sized spinel powders showed that samples beyond 24 hours milling time required additional dispersant due to the increase in surface area of the particles. The optimum dispersant dosage was evaluated based on the apparent viscosity, and the presence of flocs was estimated by fitting the results into the Herschel-Bulkley equation. Based on the results from PSD, sedimentation test, and flow curve analysis, 40 wt.% dispersant with respect to the powder was chosen as the optimal dosage. The optimum solid content of 30 wt.% with 10 wt.% binder was found to achieve the target viscosity of less than 10 mPa.s. After the addition of other additives final spinel ink formulation was achieved with 25 wt.% solid loading.

The final formulation for both the MCO and MCF inks exhibited shear thinning behaviour with the maximum particle size within the limits of the inkjet printer requirements (< 2μm). The

rheological behaviour of the inks at higher frequencies, during the jetting process, was assessed using the PAV rheometer and revealed the viscoelastic liquid nature of the inks with the complex viscosity less than 15 mPa.s. The formulated inks with Z values 6.17 and 4.77 for MCO and MCF inks, respectively, fell within the printable regime for the DOD mode of printing according to the calculated Re-We space parameter. The formulated inks were printed over steel substrates successfully without visible defects.

The ink formulation route proposed can be used to develop inkjet inks specifically with respect to different inkjet printer requirements. The ball milling-based procedure allows investigating different ink components and studying their effect on physio-chemical properties of the inkjet ink. The novel formulation of aqueous based spinel inkjet inks for an electro-magnetic printer and their printability on SOFC metallic interconnect substrate was demonstrated successfully and opens up pathways to many potential uses in coating of metallic components, especially for corrosive and high temperature applications. The performance of the inkjet printed spinel layers as a protective layer will be evaluated using high-temperature tests such as oxidation test and area-specific resistance measurements in the further study.

Acknowledgements

This work was supported by the FCH JU within the EU H2020 framework via the project SCORED 2:0 under contract no. 325331, and by EPSRC (UK) under contract EP/L015749/1. The authors wish to acknowledge the European Commission and the UK Engineering and Physical Sciences Research Council (EP/M014304/1) for financial support. The authors would like to thank Dr. Rumen Tomov and Professor. Vasant Kumar, Department of Materials Science and Metallurgy, University of Cambridge for their support through granting access to the printing facility.

References

[1] S. Elangovan, S. Balagopal, M. Timper, I. Bay, D. Larsen, J. Hartvigsen, Evaluation of Ferritic Stainless Steel for Use as Metal Interconnects for Solid Oxide Fuel Cells, J. Mater. Eng. Perform. 13 (2004) 265–273. doi:10.1361/10599490419153.

[2] W.Z. Zhu, S.C. Deevi, Development of interconnect materials for solid oxide fuel cells, Mater. Sci. Eng. A. 348 (2003) 227–243. doi:10.1016/S0921-5093(02)00736-0.

[3] Z. Yang, K.S. Weil, D.M. Paxton, J.W. Stevenson, Selection and Evaluation of Heat-Resistant Alloys for SOFC Interconnect Applications, J. Electrochem. Soc. 150 (2003) A1188. doi:10.1149/1.1595659.

[4] P. Kofstad, R. Bredesen, High temperature corrosion in SOFC environments, Solid State Ionics. 52 (1992) 69–75. doi:10.1016/0167-2738(92)90092-4.

[5] W.Z. Zhu, S.C. Deevi, Opportunity of metallic interconnects for solid oxide fuel cells: A status on contact resistance, Mater. Res. Bull. 38 (2003) 957–972. doi:10.1016/S0025-5408(03)00076-X.

[6] N. Mahato, A. Banerjee, A. Gupta, S. Omar, K. Balani, Progress in material selection for solid oxide fuel cell technology: A review, Prog. Mater. Sci. 72 (2015) 141–337. doi:10.1016/J.PMATSCI.2015.01.001.

[7] K. Kendall, M. Kendall, L. Niewolak, F. Tietz, W.J. Quadakkers, Interconnects, Academic Press (second edition), 2016. doi:10.1016/B978-0-12-410453-2.00007-5.

[8] Y.-Z. Hu, S.-W. Yao, C.-X. Li, C.-J. Li, S.-L. Zhang, Influence of pre-reduction on microstructure homogeneity and electrical properties of APS Mn1.5Co1.5O4 coatings for SOFC interconnects, Int. J. Hydrogen Energy. 42 (2017) 27241–27253. doi:10.1016/J.IJHYDENE.2017.09.073.

[9] A. Masi, M. Bellusci, S.J. McPhail, F. Padella, P. Reale, J.E. Hong, R. Steinberger-Wilckens, M. Carlini, The effect of chemical composition on high temperature behaviour of Fe and Cu doped Mn-Co spinels, Ceram. Int. 43 (2017) 2829–2835. doi:10.1016/j.ceramint.2016.11.135.

[10] A. Masi, M. Bellusci, S.J. McPhail, F. Padella, P. Reale, J.-E. Hong, R. Steinberger-

Wilckens, M. Carlini, Cu-Mn-Co oxides as protective materials in SOFC technology: The effect of chemical composition on mechanochemical synthesis, sintering behaviour, thermal expansion and electrical conductivity, J. Eur. Ceram. Soc. 37 (2017) 661–669. doi:10.1016/J.JEURCERAMSOC.2016.09.025.

[11] Z. Yang, G.G. Xia, X.H. Li, J.W. Stevenson, (Mn,Co)3O4 spinel coatings on ferritic stainless steels for SOFC interconnect applications, Int. J. Hydrogen Energy. 32 (2007) 3648–3654. doi:10.1016/j.ijhydene.2006.08.048.

[12] B. Talic, S. Molin, K. Wiik, P.V. Hendriksen, H.L. Lein, Comparison of iron and copper doped manganese cobalt spinel oxides as protective coatings for solid oxide fuel cell interconnects, J. Power Sources. 372 (2017) 145–156. doi:10.1016/J.JPOWSOUR.2017.10.060.

[13] X. Chen, P.Y. Hou, C.P. Jacobson, S.J. Visco, L.C. De Jonghe, Protective coating on stainless steel interconnect for SOFCs: Oxidation kinetics and electrical properties, Solid State Ionics. 176 (2005) 425–433. doi:10.1016/j.ssi.2004.10.004.

[14] Y. Larring, T. Norby, Functional Layers Between Plansee Metallic Interconnect (Cr-5 wt% Fe-1 wt% Y 2 O 3) and Ceramic (La0. 85Sr0. 15) 0.91 MnO3 Cathode Materials for Solid Oxide, J. Electrochem. Soc. 147 (2000) 3251–3256. http://jes.ecsdl.org/content/147/9/3251.short.

[15] M.Y. Yoon, E.J. Lee, R.H. Song, H.J. Hwang, Preparation and properties of a MnCo 2O 4 for ceramic interconnect of solid oxide fuel cell via glycine nitrate process, Met. Mater. Int. 17 (2011) 1039–1043. doi:10.1007/s12540-011-6025-5.

[16] Z. Yang, G. Xia, S.P. Simner, J.W. Stevenson, Thermal Growth and Performance of Manganese Cobaltite Spinel Protection Layers on Ferritic Stainless Steel SOFC Interconnects, J. Electrochem. Soc. 152 (2005) A1896. doi:10.1149/1.1990462.

[17] Z. Yang, G. Xia, C. Wang, Z. Nie, J. Templeton, J. Stevenson, P. Singh, Investigation of AISI 441 Ferritic Stainless Steel and Development of Spinel Coatings for SOFC Interconnect Applications, Top. Report, Pacific Northwest Natl. Lab. PNNL-17568. (2008).

[18] S.T. Hashemi, A.M. Dayaghi, M. Askari, P.E. Gannon, Sol-gel synthesis of Mn1.5Co1.5O4 spinel nano powders for coating applications, Mater. Res. Bull. 102

(2018) 180–185. doi:10.1016/J.MATERRESBULL.2018.02.040.

[19] S. Molin, P. Jasinski, L. Mikkelsen, W. Zhang, M. Chen, P.V. Hendriksen, Low temperature processed MnCo2O4 and MnCo1.8Fe0.2O4 as effective protective coatings for solid oxide fuel cell interconnects at 750 °C, J. Power Sources. 336 (2016) 408–418. doi:10.1016/j.jpowsour.2016.11.011.

[20] B. Talic, P.V. Hendriksen, K. Wiik, H.L. Lein, Thermal expansion and electrical conductivity of Fe and Cu doped MnCo2O4 spinel, Solid State Ionics. 326 (2018) 90–99. doi:10.1016/J.SSI.2018.09.018.

[21] T. Dippong, E. Andrea, L. Oana, C. Firuta, G. Dana, G. Borodi, T. Dippong, E.A. Levei, Thermal behavior of Ni , Co and Fe succinates embedded in silica matrix, J. Therm. Anal. Calorim. 136 (2019) 1587–1596. doi:10.1007/s10973-019-08117-8.

[22] N. Shaigan, W. Qu, D.G. Ivey, W. Chen, A review of recent progress in coatings, surface modifications and alloy developments for solid oxide fuel cell ferritic stainless steel interconnects, J. Power Sources. 195 (2010) 1529–1542. doi:10.1016/j.jpowsour.2009.09.069.

[23] J.C.W. Mah, A. Muchtar, M.R. Somalu, M.J. Ghazali, Metallic interconnects for solid oxide fuel cell: A review on protective coating and deposition techniques, Int. J. Hydrogen Energy. 42 (2017) 9219–9229. doi:10.1016/J.IJHYDENE.2016.03.195.

[24] E. Venezia, M. Viviani, S. Presto, V. Kumar, R.I. Tomov, Inkjet Printing Functionalization of SOFC LSCF Cathodes, Nanomaterials. 9 (2019) 654. doi:10.3390/nano9040654.

[25] J. Castrejon-Pita, W. Baxter, Future , Opportunities and Challenges of Inkjet Technologies, At. Sprays. (2013) 1–13. doi:10.1615/AtomizSpr.2013007653.

[26] B. Tawiah, E.K. Howard, B.K. Asinyo, The Chemistry of Inkjet Inks for Digital Textile Printing - Review, Int. J. Manag. Inf. Technol. Eng. 4 (2016) 61–78.

[27] A. Kosmala, R. Wright, Q. Zhang, P. Kirby, Synthesis of silver nano particles and fabrication of aqueous Ag inks for inkjet printing, Mater. Chem. Phys. 129 (2011) 1075–1080. doi:10.1016/j.matchemphys.2011.05.064.

[28] M. Romagnoli, M. Lassinantti Gualtieri, M. Cannio, F. Barbieri, R. Giovanardi, Preparation of an aqueous graphitic ink for thermal drop-on-demand inkjet printing,

Mater. Chem. Phys. 182 (2016) 263–271. doi:10.1016/J.MATCHEMPHYS.2016.07.031.

[29] M. Özkan, K. Dimic-Misic, A. Karakoc, S.G. Hashmi, P. Lund, T. Maloney, J. Paltakari, Rheological characterization of liquid electrolytes for drop-on-demand inkjet printing, Org. Electron. 38 (2016) 307–315. doi:10.1016/J.ORGEL.2016.09.001.

[30] X. Liu, T.J. Tarn, F. Huang, J. Fan, Recent advances in inkjet printing synthesis of functional metal oxides, Particuology. 19 (2015) 1–13. doi:10.1016/j.partic.2014.05.001.

[31] G.L. Güngör, A. Kara, M. Blosi, D. Gardini, G. Guarini, C. Zanelli, M. Dondi, Micronizing ceramic pigments for inkjet printing: Part I. Grindability and particle size distribution, Ceram. Int. 41 (2015) 6498–6506. doi:10.1016/j.ceramint.2015.01.093.

[32] V. Esposito, C. Gadea, J. Hjelm, D. Marani, Q. Hu, K. Agersted, S. Ramousse, S.H. Jensen, Fabrication of thin yttria-stabilized-zirconia dense electrolyte layers by inkjet printing for high performing solid oxide fuel cells, J. Power Sources. 273 (2015) 89–95. doi:10.1016/J.JPOWSOUR.2014.09.085.

[33] S.H. Rahul, K. Balasubramanian, S. Venkatesh, Optimizing inkjet printing process to fabricate thick ceramic coatings, Ceram. Int. 43 (2017) 4513–4519. doi:10.1016/J.CERAMINT.2016.12.103.

[34] Z. Chen, N. Brandon, Inkjet printing and nanoindentation of porous alumina multilayers, Ceram. Int. 42 (2016) 8316–8324. doi:10.1016/j.ceramint.2016.02.045.

[35] W.Y. Padrón-Hernández, M.C. Ceballos-Chuc, D. Pourjafari, G. Oskam, J.C. Tinoco, A.G. Martínez-López, G. Rodríguez-Gattorno, Stable inks for inkjet printing of TiO2 thin films, Mater. Sci. Semicond. Process. 81 (2018) 75–81. doi:10.1016/J.MSSP.2018.03.015.

[36] M. Bissannagari, T.H. Kim, J.G. Yook, J. Kim, All inkjet-printed flexible wireless power transfer module: PI/Ag hybrid spiral coil built into 3D NiZn-ferrite trench structure with a resonance capacitor, Nano Energy. 62 (2019) 645–652. doi:10.1016/j.nanoen.2019.05.075.

[37] J. Izdebska, S. Thomas, A. Pekarovicova, V. Husovska, 3 – Printing Ink Formulations, in: Print. Polym., 2016: pp. 41–55. doi:10.1016/B978-0-323-37468-2.00003-8.

[38] X. Li, Y. Zhao, J. Yu, Q. Liu, R. Chen, H. Zhang, D. Song, R. Li, J. Liu, J. Wang, Layer-by-layer inkjet printing GO film and Ag nanoparticles supported nickel cobalt layered double hydroxide as a flexible and binder-free electrode for supercapacitors, J. Colloid Interface Sci. 557 (2019) 691–699. doi:10.1016/j.jcis.2019.09.063.

[39] W. Zi, Z. Jin, S. Liu, B. Xu, Flexible perovskite solar cells based on green, continuous roll-to-roll printing technology, J. Energy Chem. 27 (2018) 971–989. doi:10.1016/j.jechem.2018.01.027.

[40] S. Ganesan, S. Mehta, D. Gupta, Fully printed organic solar cells - A review of techniques, challenges and their solutions, Opto-Electronics Rev. 27 (2019) 298–320. doi:10.1016/j.opelre.2019.09.002.

[41] P. Sundriyal, S. Bhattacharya, Inkjet-Printed Sensors on Flexible Substrates, (2018) 89–113. doi:10.1007/978-981-10-7751-7_5.

[42] D. Lv, W. Chen, W. Shen, M. Peng, X. Zhang, R. Wang, L. Xu, W. Xu, W. Song, R. Tan, Enhanced flexible room temperature ammonia sensor based on PEDOT: PSS thin film with FeCl3 additives prepared by inkjet printing, Sensors Actuators, B Chem. 298 (2019). doi:10.1016/j.snb.2019.126890.

[43] G. Rosati, M. Ravarotto, M. Sanavia, M. Scaramuzza, A. De Toni, A. Paccagnella, Inkjet sensors produced by consumer printers with smartphone impedance readout, Sens. Bio-Sensing Res. 26 (2019). doi:10.1016/j.sbsr.2019.100308.

[44] S.S. Yerneni, T.L. Whiteside, L.E. Weiss, P.G. Campbell, Bioprinting exosome-like extracellular vesicle microenvironments, Bioprinting. 13 (2019). doi:10.1016/j.bprint.2019.e00041.

[45] K. Li, W. Chen, J. Liu, H. Li, N. Qi, Y. Liu, Research on the spreading characteristics of biodegradable ethyl cyanoacrylate droplet of a piezoelectric inkjet, Sensors Actuators, A Phys. 302 (2020). doi:10.1016/j.sna.2019.111810.

[46] K. Sen, A. Manchanda, T. Mehta, A.W.K. Ma, B. Chaudhuri, Formulation design for inkjet-based 3D printed tablets, Int. J. Pharm. 584 (2020). doi:10.1016/j.ijpharm.2020.119430.

[47] C. Wang, R.I. Tomov, R.V. Kumar, B.A. Glowacki, Inkjet printing of gadolinium-doped ceria electrolyte on NiO-YSZ substrates for solid oxide fuel cell applications, J.

Mater. Sci. 46 (2011) 6889–6896. doi:10.1007/s10853-011-5653-y.

[48] R.I. Tomov, R. Duncan, M. Krauz, R. Vasant Kumar, B.A. Glowacki, Inkjet printing and inkjet infiltration of functional coatings for SOFCs fabrication, in: M. Filipowicz, M. Dudek, T. Olkuski, K. Styszko (Eds.), E3S Web Conf., 2016: p. 00098. doi:10.1051/e3sconf/20161000098.

[49] R.I. Tomov, M. Krauz, A. Tluczek, R. Kluczowski, V. V. Krishnan, K. Balasubramanian, R. V. Kumar, B.A. Glowacki, Vacuum-sintered stainless steel porous supports for inkjet printing of functional SOFC coatings, Mater. Renew. Sustain. Energy. 4 (2015) 1–11. doi:10.1007/s40243-015-0056-7.

[50] Z. Chen, J. Ouyang, W. Liang, Z. Yan, F. Stadler, C. Lao, Development and characterizations of novel aqueous-based LSCF suspensions for inkjet printing, Ceram. Int. 44 (2018) 13381–13388. doi:10.1016/J.CERAMINT.2018.04.174.

[51] S. Kittaka, T. Morimoto, Isoelectric point of metal oxides and binary metal oxides having spinel structure, J. Colloid Interface Sci. 75 (1980) 398–403. doi:10.1016/0021-9797(80)90464-6.

[52] D. Houivet, E. Fallah, J. Haussonne, Dispersion and Grinding of Oxide Powders into an Aqueous Slurry, 28 (2002) 321–328.

[53] B.P. Singh, S. Bhattacharjee, L. Besra, D.K. Sengupta, Electrokinetic and adsorption studies of alumina suspensions using Darvan C as dispersant, J. Colloid Interface Sci. 289 (2005) 592–596. doi:10.1016/J.JCIS.2005.03.096.

[54] L. Jin, X. Mao, S. Wang, M. Dong, Optimization of the rheological properties of yttria suspensions, Ceram. Int. 35 (2009) 925–927. doi:10.1016/j.ceramint.2008.03.009.

[55] Malvern Instruments Ltd., Zeta potential: An Introduction in 30 minutes, 2011. https://www.malvernpanalytical.com/en/learn/knowledge-center/technical-notes/TN101104ZetaPotentialIntroduction (accessed July 12, 2019).

[56] G.L. Güngör, A. Kara, D. Gardini, M. Blosi, M. Dondi, C. Zanelli, Ink-jet printability of aqueous ceramic inks for digital decoration of ceramic tiles, Dye. Pigment. 127 (2016) 148–154. doi:10.1016/J.DYEPIG.2015.12.018.

[57] G. Suárez, M.P. Albano, L.B. Garrido, E.F. Aglietti, Dispersion of concentrated aqueous yttria-stabilized zirconia with ammonium polyacrylate, Ceram. Int. 33 (2007)

925–929. doi:10.1016/J.CERAMINT.2006.02.003.

[58] C. Miao, R. Shen, M. Wang, S.N. Shafrir, H. Yang, S.D. Jacobs, Rheology of aqueous magnetorheological fluid using dual oxide-coated carbonyl iron particles, J. Am. Ceram. Soc. 94 (2011) 2386–2392. doi:10.1111/j.1551-2916.2011.04423.x.

[59] M. Michálek, G. Blugan, T. Graule, J. Kuebler, Comparison of aqueous and non-aqueous tape casting of fully stabilized ZrO2suspensions, Powder Technol. 274 (2015) 276–283. doi:10.1016/j.powtec.2015.01.036.

[60] A. Karppinen, A.H. Vesterinen, T. Saarinen, P. Pietikäinen, J. Seppälä, Effect of cationic polymethacrylates on the rheology and flocculation of microfibrillated cellulose, Cellulose. 18 (2011) 1381–1390. doi:10.1007/s10570-011-9597-9.

[61] D. Gardini, M. Deluca, M. Nagliati, C. Galassi, Flow properties of PLZTN aqueous suspensions for tape casting, Ceram. Int. 36 (2010) 1687–1696. doi:10.1016/J.CERAMINT.2010.03.011.

[62] Z. Zhou, P.J. Scales, D. V Boger, Chemical and physical control of the rheology of concentrated metal oxide suspensions, Chem. Eng. Sci. 56 (2001) 2901–2920. doi:10.1016/S0009-2509(00)00473-5.

[63] A.U. Khan, B.J. Briscoe, P.F. Luckham, Interaction of binders with dispersant stabilised alumina suspensions, Colloids Surfaces A Physicochem. Eng. Asp. 161 (2000) 243–257. doi:10.1016/S0927-7757(99)00374-X.

[64] P.P. Nampi, S. Kume, Y. Hotta, K. Watari, M. Itoh, H. Toda, A. Matsutani, The effect of polyvinyl alcohol as a binder and stearic acid as an internal lubricant in the formation, and subsequent sintering of spray-dried alumina, Ceram. Int. 37 (2011) 3445–3450. doi:10.1016/J.CERAMINT.2011.05.149.

[65] J. A.Lewis, Colloidal processing of ceramics and composites, Jounal Am. Ceram. Scociety. 111 (2000) 246–253. doi:10.1179/1743676111Y.0000000075.

[66] W.D. Teng, M.J. Edirisinghe, J.R.G. Evans, Optimization of Dispersion and Viscosity of a Ceramic Jet Printing Ink, J. Am. Ceram. Soc. 80 (2005) 486–494. doi:10.1111/j.1151-2916.1997.tb02855.x.

[67] M. Victoria, A. Umaran, R. Labandera, Aqueous Dispersion of Red Clay-based Ceramic Powder with the Addition of Starch, 16 (2013) 375–384. doi:10.1590/S1516-

14392013005000002.

[68] S.D. Hoath, I.M. Hutchings, G.D. Martin, T.R. Tuladhar, M.R. Mackley, D. Vadillo, Links Between Ink Rheology, Drop-on-Demand Jet Formation, and Printability, J. Imaging Sci. Technol. 53 (2009) 041208. doi:10.2352/j.imagingsci.technol.2009.53.4.041208.

[69] K. Woo, D. Jang, Y. Kim, J. Moon, Relationship between printability and rheological behavior of ink-jet conductive inks, Ceram. Int. 39 (2013) 7015–7021. doi:10.1016/j.ceramint.2013.02.039.

[70] D.C. Vadillo, T.R. Tuladhar, A.C. Mulji, M.R. Mackley, The rheological characterization of linear viscoelasticity for ink jet fluids using piezo axial vibrator and torsion resonator rheometers, J. Rheol. (N. Y. N. Y). 54 (2010) 781–795. doi:10.1122/1.3439696.

[71] J.E. Fromm, Numerical Calculation of the Fluid Dynamics of Drop-on-Demand Jets, IBM J. Res. Dev. 28 (1984) 322–333. doi:10.1147/rd.283.0322.

[72] N. Reis, B. Derby, Ink jet deposition of ceramic suspensions: Modelling and experiments of droplet formation, Mater. Res. Soc. Symp. - Proc. 624 (2000) 65–70. doi:10.1557/proc-625-117.

[73] B. Derby, Inkjet printing ceramics: From drops to solid, J. Eur. Ceram. Soc. 31 (2011) 2543–2550. doi:10.1016/j.jeurceramsoc.2011.01.016.

[74] B. Derby, N. Reis, Inkjet Printing of Highly Loaded Particulate Suspensions, MRS Bull. 28 (2003) 815–818. doi:10.1557/mrs2003.230.

[75] R.I. Tomov, M. Krauz, J. Jewulski, S.C. Hopkins, J.R. Kluczowski, D.M. Glowacka, B.A. Glowacki, Direct ceramic inkjet printing of yttria-stabilized zirconia electrolyte layers for anode-supported solid oxide fuel cells, J. Power Sources. 195 (2010) 7160–7167. doi:10.1016/j.jpowsour.2010.05.044.

List of Tables:

Table 1: Dynamic viscosity of the ink suspensions measured at low and high shear rate for varying dispersant dosage

Ink	Shear rate (1/s)	Dispersant dosage				
		5 wt.%	10 wt.%	20 wt.%	30wt.%	40wt.%
MCO	1.00	14.59	24.67	16.42	13.57	11.05
	1000	2.06	2.77	3.20	3.62	4.24
MCF	1.00	60.29	65.83	41.22	37.42	15.90
	1000	6.49	5.32	4.08	3.42	3.61

Table 2: Dynamic viscosity of the inks with different binder concentration at low and high dispersant dosage.

Ink	Shear rate (1/s)	Viscosity (mPa.s)					
		Low dispersant dosage (5 wt.%)			High dispersant dosage (40 wt.%)		
		5wt.% B	10wt.%B	15wt.%B	5wt.%B	10wt.%B	15wt.%B
MCO	1.00	63.94	91.44	560.29	24.42	20.26	36.43
	1000	6.09	16.56	26.81	5.48	6.86	10.26
MCF	1.00	16.12	62.87	104.45	25.88	69.57	82.65
	1000	4.26	8.54	13.39	4.37	6.83	9.21

Table 3: Dynamic viscosity of the ink suspensions with varying solid loading.

Ink	Shear rate (1/s)	Solid loading		
		30 wt%	35 wt.%	40 wt.%
MCO	1.00	17.09	27.60	50.27
	1000	7.58	7.26	15.51
MCF	1.00	33.50	65.50	-
	1000	10.75	15.89	-

Table 4: Composition of the MCO and MCF inks with optimal amount of dispersant, binder, solid loading, and other additives.

Component	Amount (wt.%)
DI	35.53
Powder	25.38
Dispersant	10.15
Binder (solution)	18.27
PEG +Glycerol	10.15
Surfactant	0.25
Antifoam	0.25

Table 5: PSD of MCO and MCF final ink composition measured on day 0 and day 7

Ink	Day 0			Day 7		
	d_{50} (µm)	**d_{90} (µm)**	**Span**	**d_{50} (µm)**	**d_{90} (µm)**	**Span**
MCO	0.68 ±0.010	1.29 ± 0.017	1.44 ±0.001	0.87 ±0.005	1.50 ±0.012	1.24 ±0.002
MCF	0.50 ±0.002	1.05± 0.003	1.64±0.003	0.78 ±0.002	1.47 ± 0.006	1.46 ±0.004

Table 6: Physical properties of the inks

Ink	**η (mPa.s) at 1000 s^{-1}**	**γ* (dyne/cm)**	**ρ (g/cc)**	**Re**	**We**	**Oh**	**Z=1/Oh**
MCO	10	35.2	1.2	38.9	39.8	0.16	6.17
MCF	13	32.9	1.3	32.4	46.0	0.21	4.77

** Surface tension of the inks were measured using Wilhelmy plate method.*

List of Figures:

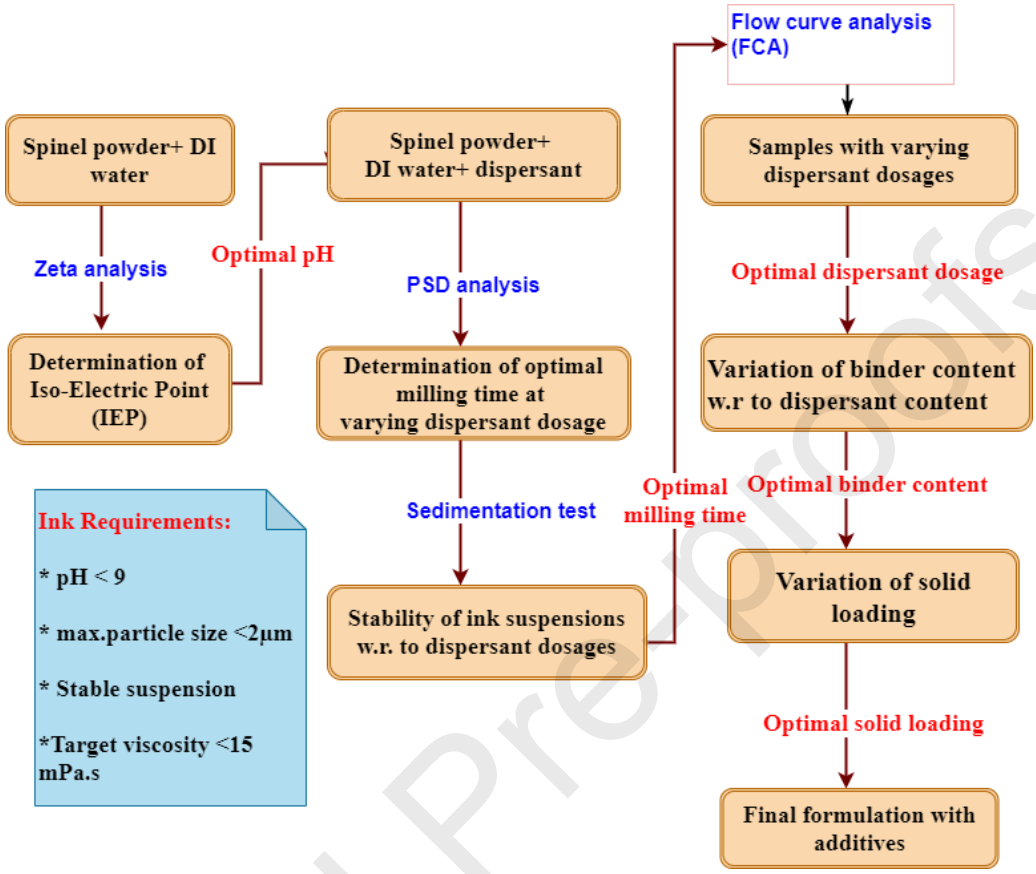

Figure 1: Schematic of the ink formulation route.

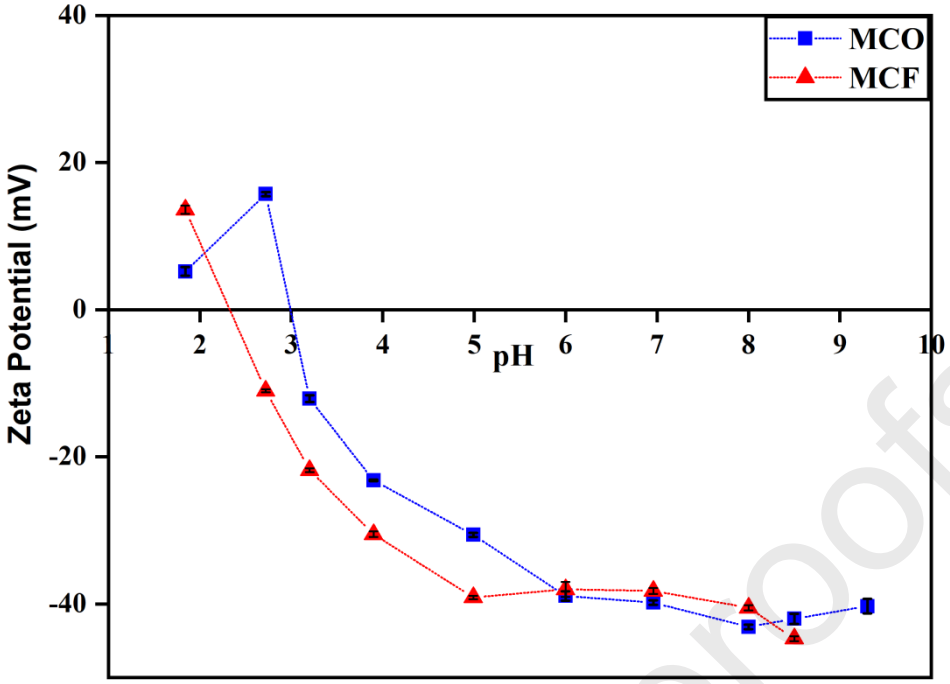

Figure 2: ISE curves for MCO and MCF inks. The iso-electric point of both the spinel inks is in the pH range 2.3 to 3.0.

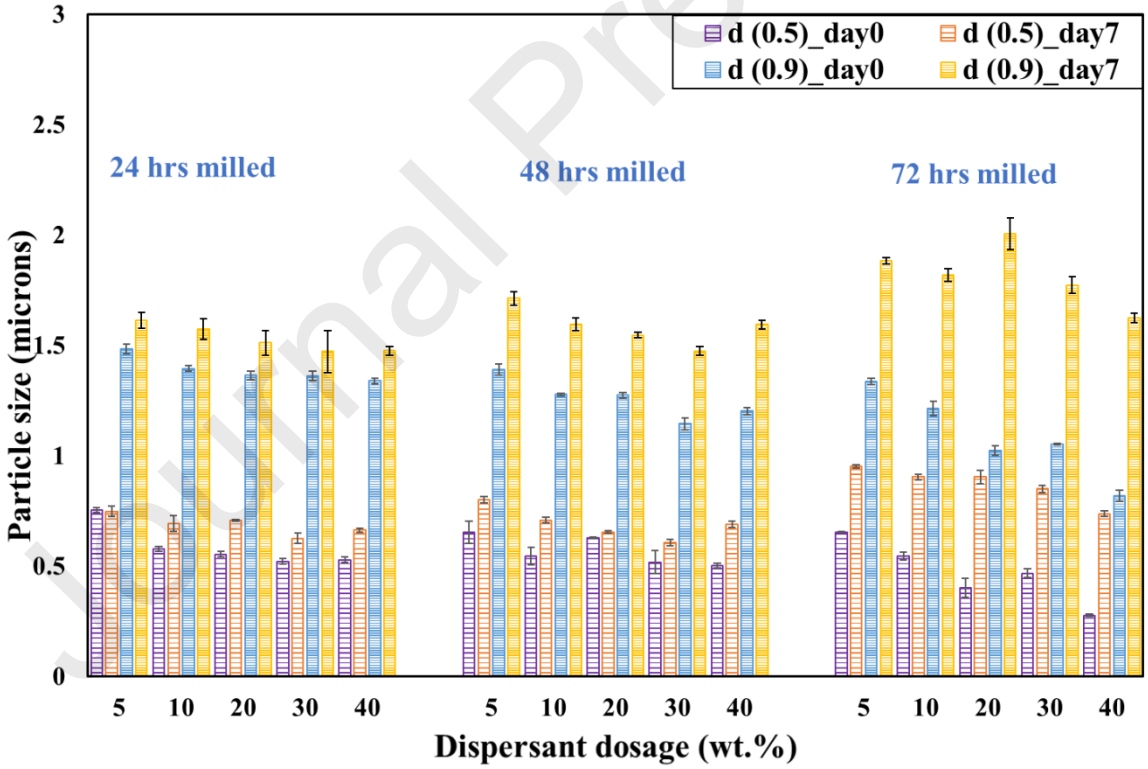

Figure 3: Evolution of d_{50} and d_{90} values of MCO ink suspension milled for 24, 48 and 72 hrs with different dispersant dosages.

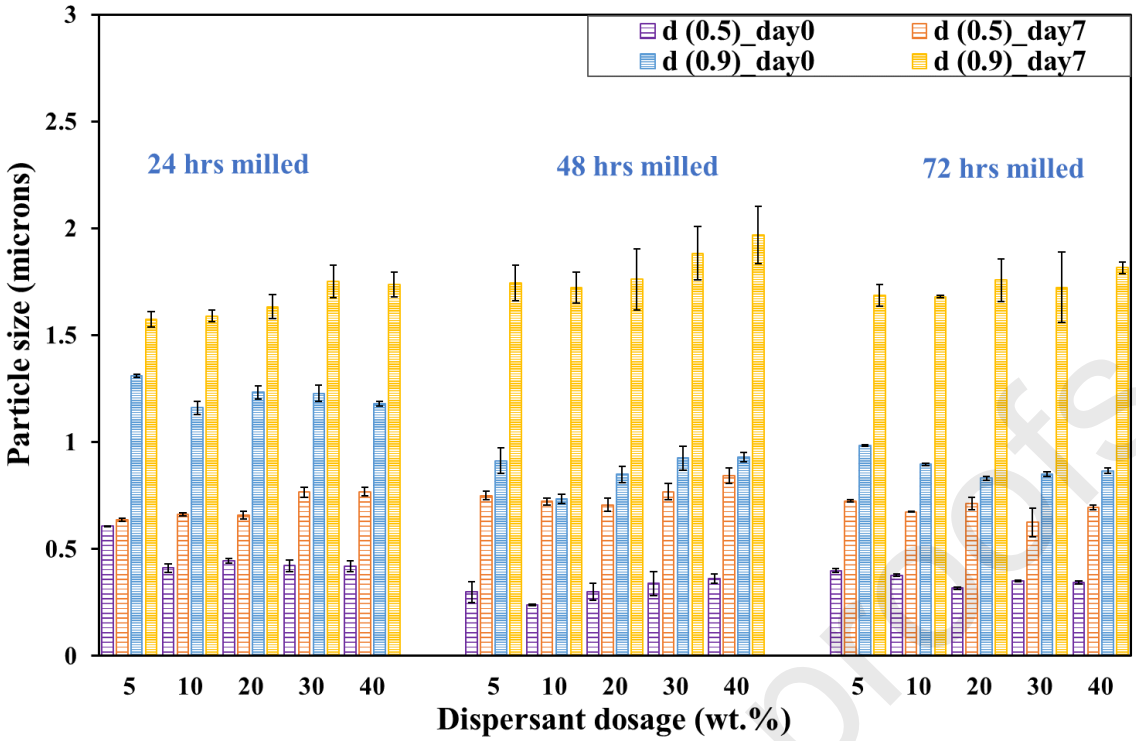

Figure 4: Evolution of d_{50} and d_{90} values of MCF ink suspension milled for 24, 48 and 72 hrs with different dispersant dosages.

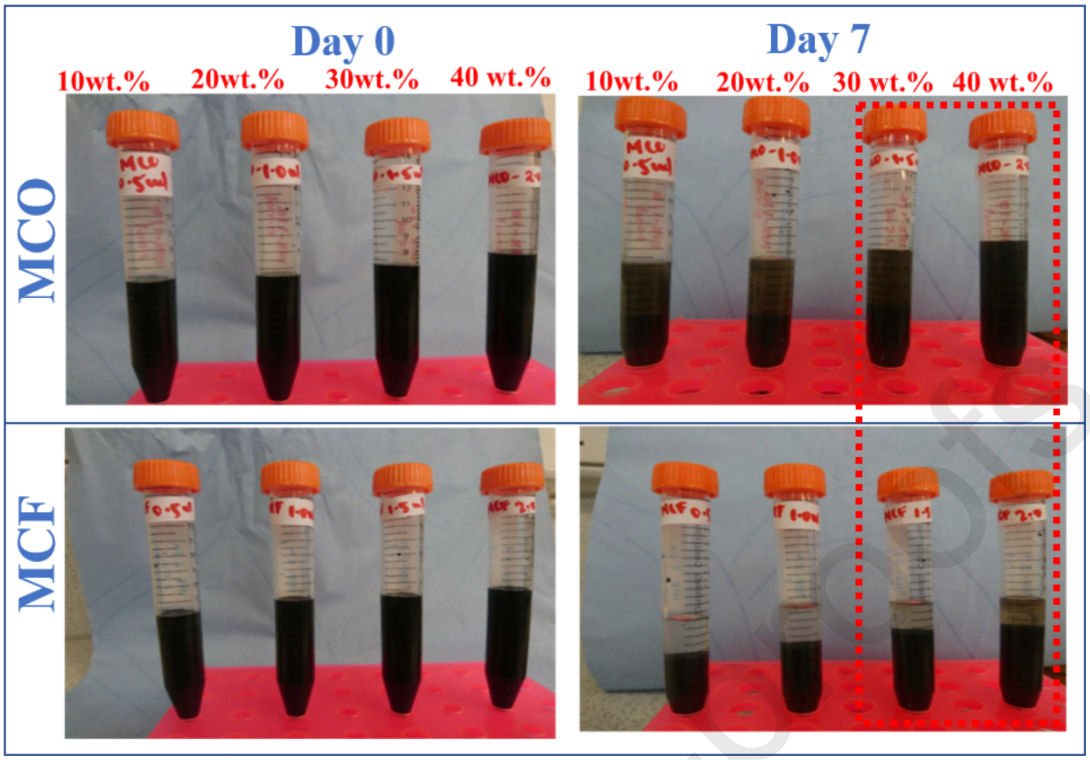

Figure 5: Sedimentation test - MCO and MCF ink suspensions milled for 24 hours with varying dispersant dosages. 30 and 40wt.% suspensions displayed better stability relative to other dosages, turbid supernatant shows the dispersed particles in the suspension.

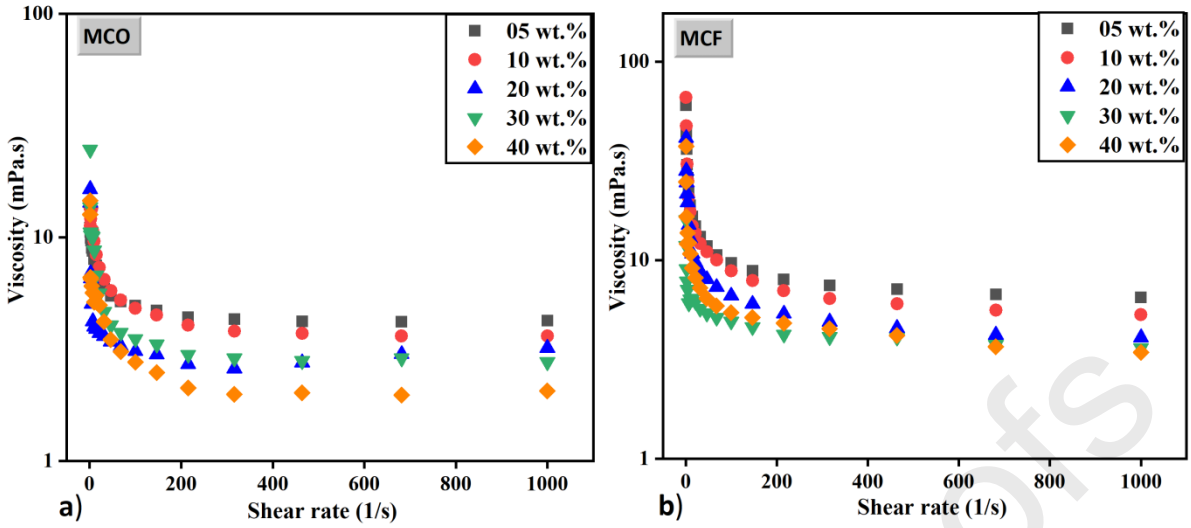

Figure 6: Flow curve of MCO inks (a) and MCF inks (b) at the shear rate (1-1000 s^{-1}) with varying dispersant dosage.

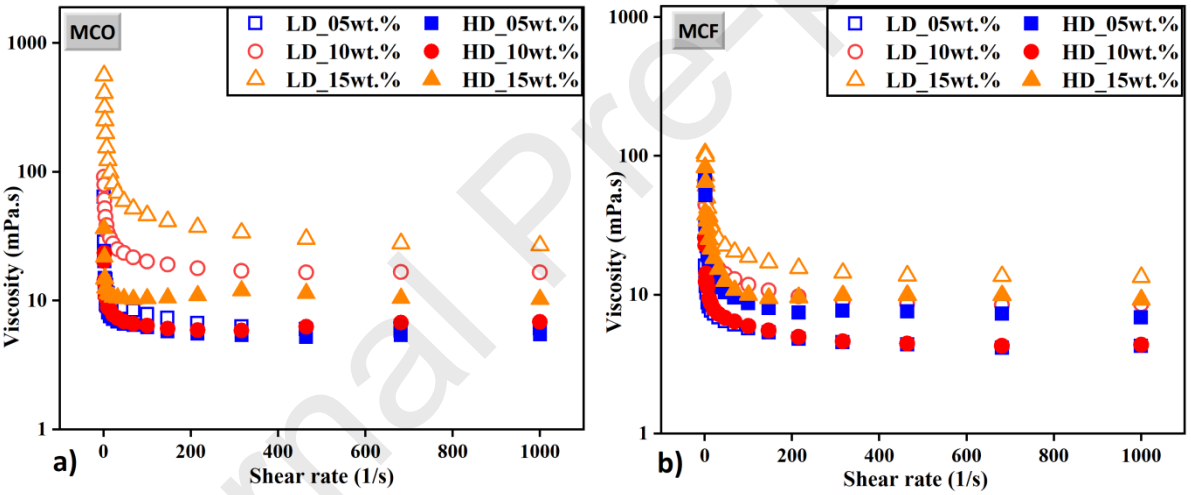

Figure 7: Flow curve of MCO inks (a) and MCF inks (b) at the shear rate (1-1000 s^{-1}) with varying binder concentration at low and high dispersant dosage.

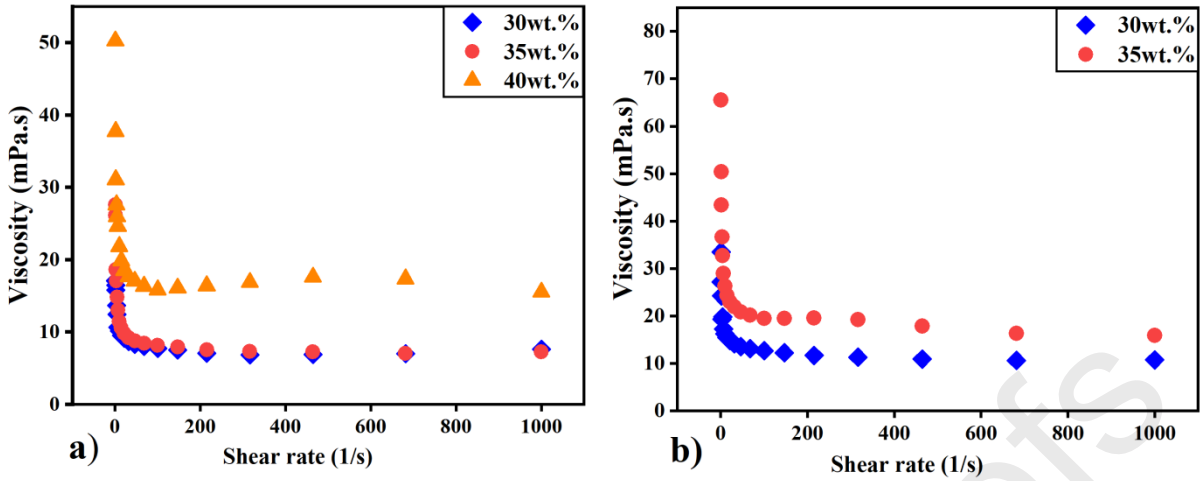

Figure 8: Flow curve of MCO inks (a) and MCF inks (b) at the shear rate (1-1000 s^{-1}) with different solid loading.

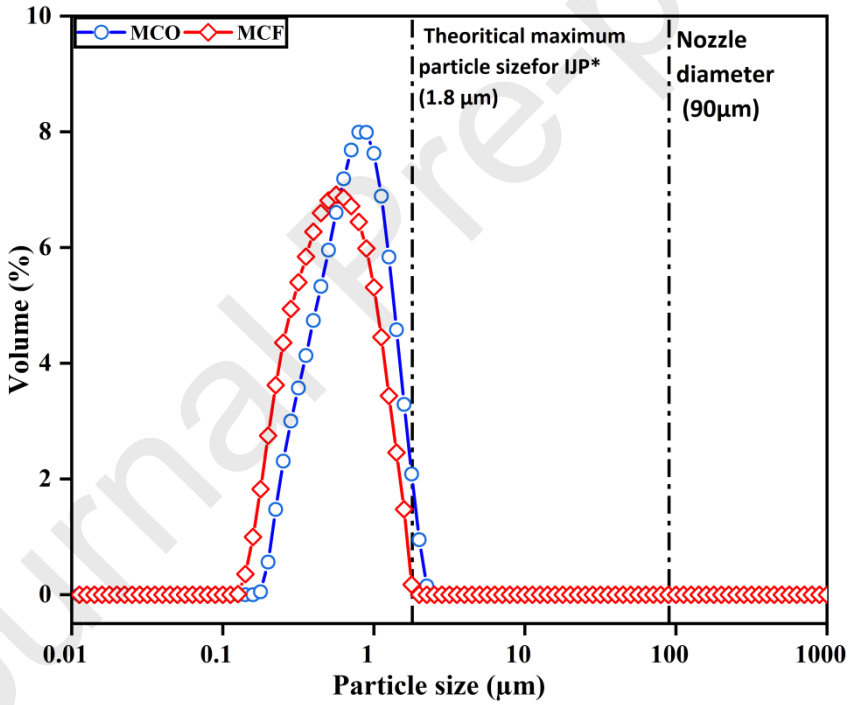

Figure 9: PSD of the MCO and MCF inks with the optimal composition displaying narrow distribution with no signs of agglomeration.

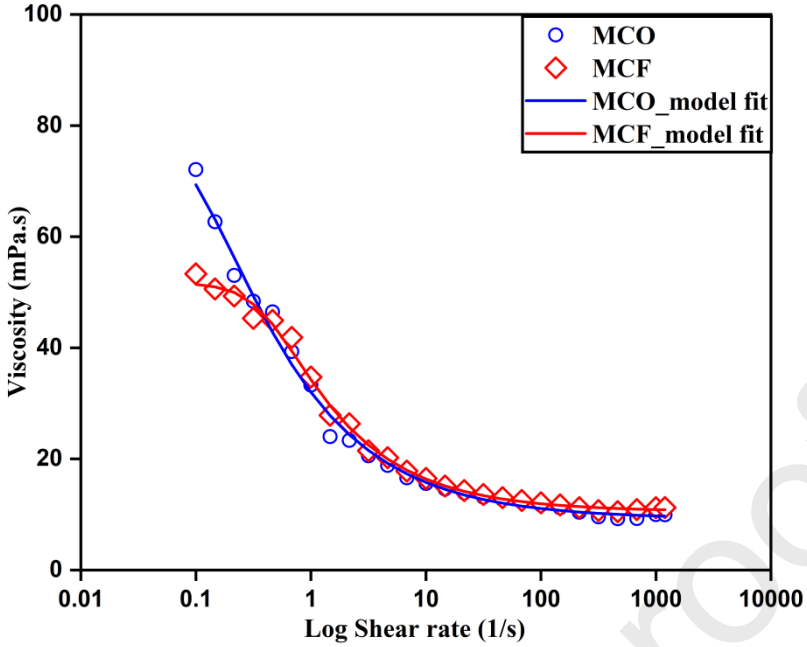

Figure 10: Flow curve of MCO and MCF inks exhibiting shear-thinning behaviour. The model fitting for both the inks is represented by the line plot, where R^2 values for MCO and MCF inks were 0.98 and 0.99.

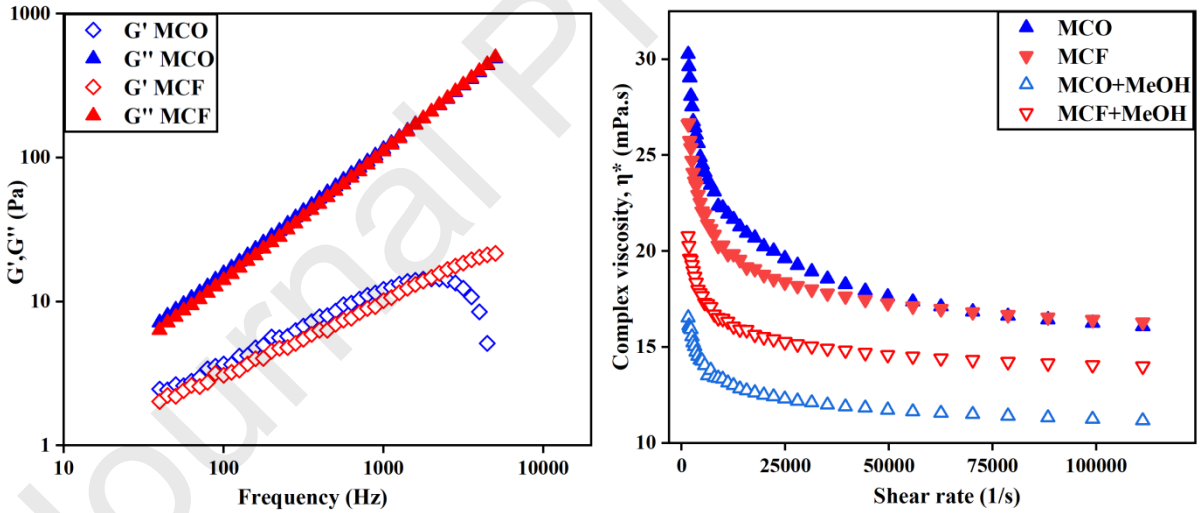

Figure 11: (a) Storage and loss moduli of MCO and MCF inks measured in the frequency range 30 Hz to 5 kHz. Both the inks displayed a viscoelastic liquid nature with dominant G'', (b) viscoelastic behaviour of the inks with and without methanol expressed by complex viscosity at shear rate.

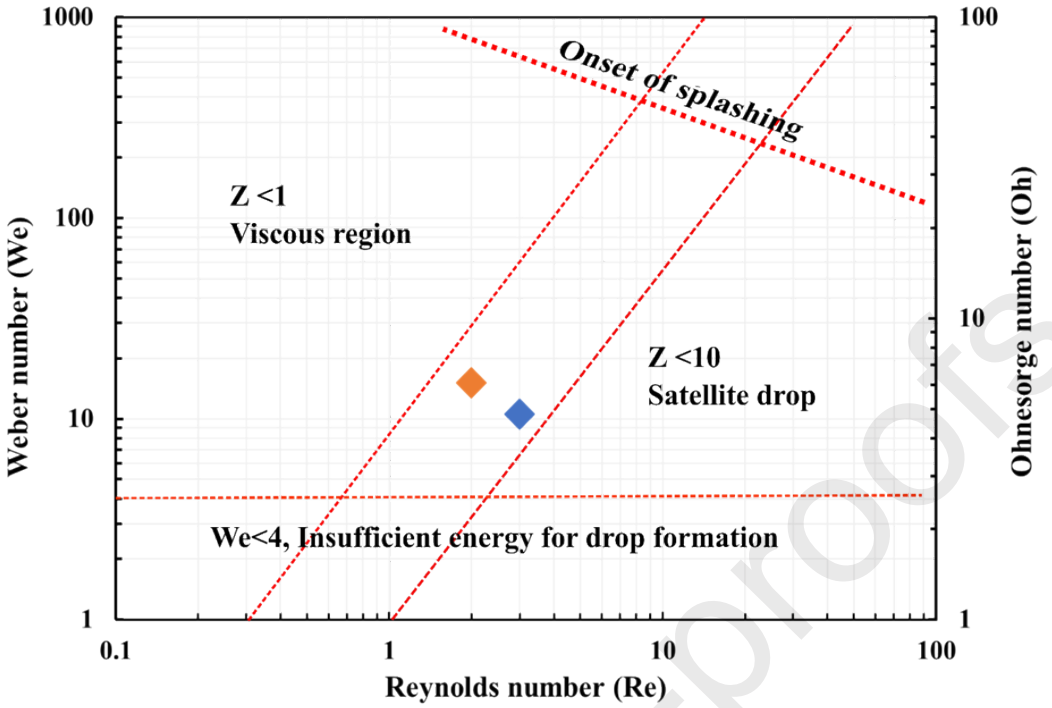

Figure 12: Re-We space parameter that defines the printing characteristics of the formulated spinel inks. The Z value for MCO (orange diamond) and MCF inks are 6.17 and 4.77, respectively.

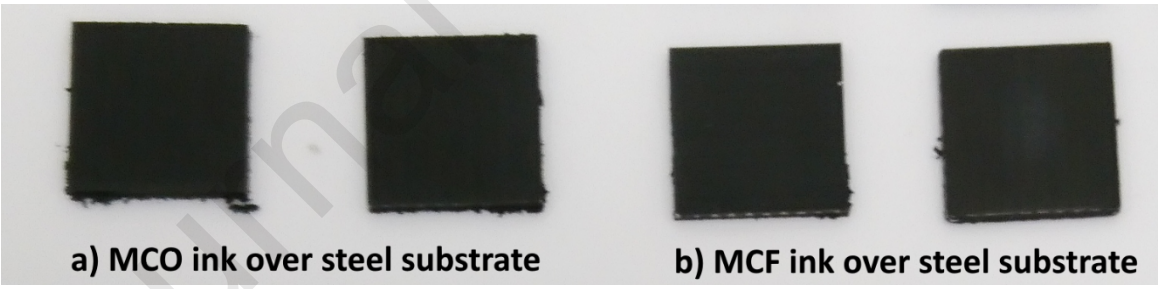

Figure 13: K41 steel substrates with MCO and MCF inks post heat-treatment process.

Credit authorship statement:

Sathish Pandiyan: Conceptualization, Methodology, Investigation, Validation, Visualization, Writing- Original draft. **Ahmad El-Kharouf:** Conceptualization, Validation, Visualization, Supervision, Writing- Review & Editing. **Robert Steinberger-Wilckens:** Conceptualization, Supervision, Writing- Review & Editing, Project administration, Funding acquisition.

Declaration of interests

☒ The authors declare that they have no known competing financial interests or personal relationships that could have appeared to influence the work reported in this paper.

☐The authors declare the following financial interests/personal relationships which may be considered as potential competing interests:

Graphical abstract

Formulation of spinel inkjet inks

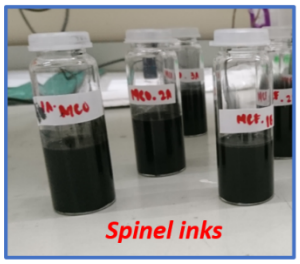

Printability of the spinel inks

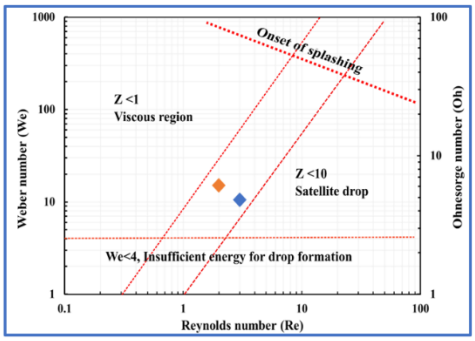

Reynolds –Weber space parameter
The Z value of the formulated inks was well within the printable region.

Inkjet printing of the spinel inks onto the steel substrate